# Antagonistic regulation of trafficking to *Caenorhabditis elegans* sensory cilia by a *Retinal Degeneration 3* homolog and retromer

Luis A. Martínez-Velázquez[a,b,c,d] and Niels Ringstad[a,b,c,d,1]

[a]Skirball Institute for Biomolecular Medicine, New York University School of Medicine, New York, NY 10016; [b]The Helen L. and Martin S. Kimmel Center for Biology and Medicine, New York University School of Medicine, New York, NY 10016; [c]Neuroscience Institute, New York University School of Medicine, New York, NY 10016; and [d]Department of Cell Biology, New York University School of Medicine, New York, NY 10016

Edited by Martin Chalfie, Columbia University, New York, NY, and approved November 29, 2017 (received for review July 11, 2017)

**Sensory neurons often possess cilia with elaborate membrane structures that are adapted to the sensory modality of the host cell. Mechanisms that target sensory transduction proteins to these specialized membrane domains remain poorly understood. Here, we show that a homolog of the human retinal dystrophy gene *Retinal Degeneration 3* (*RD3*) is a Golgi-associated protein required for efficient trafficking of a sensory receptor, the receptor-type guanylate cyclase GCY-9, to cilia in chemosensory neurons of the nematode *Caenorhabditis elegans*. The trafficking defect caused by mutation of the nematode *RD3* homolog is suppressed in vivo by mutation of key components of the retromer complex, which mediates recycling of cargo from endosomes to the Golgi. Our data show that there exists a critical balance in sensory neurons between the rates of anterograde and retrograde trafficking of cargo destined for the sensory cilium and this balance requires molecular specialization at an early stage of the secretory pathway.**

*Caenorhabditis elegans* | sensory neuron | cilium | guanylate cyclase | retinal degeneration

In many postmitotic cells, the mother centriole is repurposed to organize the primary cilium, a microtubule-based structure that protrudes from the plasma membrane (1). Mutations that affect the primary cilium cause pleiotropic phenotypes and are the root causes of a family of disorders referred to as ciliopathies. Ciliopathies cause defects in physiological homeostasis, organ development and cell function, intellectual disability, polycystic kidney disease, and sensory defects such as anosmia and blindness (2). Sensory defects caused by ciliopathies highlight the essential role for cilia in sensory neurons. Membranes of the sensory cilium are enriched with molecules that mediate sensory transduction (3). The morphology and protein composition of ciliary membranes vary between sensory neuron types. For example, vertebrate olfactory neurons are multiciliated, which increases the area of olfactory epithelium that a single cell can monitor (4). Sensory cilia of vertebrate photoreceptor neurons balloon into a dense stack of membranous disks that constitute the photoreceptor outer segment. The concentration of photopigment in outer segment membranes and their large surface area, which exceeds the surface area of the rest of the cell, contribute to the extraordinary efficiency and sensitivity of phototransduction in the vertebrate retina (5).

Sensory neurons of the nematode *Caenorhabditis elegans* are an excellent system for the study of mechanisms that generate and maintain sensory cilia. In this organism, the only cells with primary cilia are sensory neurons, and mutants with disrupted cilia are viable (6, 7). *C. elegans* sensory cilia display as much diversity in form and function as their vertebrate counterparts (7–9). The cilia of neurons that mediate chemosensation, mechanosensation, and thermosensation all have distinctive morphologies (6–10). Furthermore, *C. elegans* sensory cilia accumulate and organize proteins that function in sensory transduction pathways that are conserved between nematodes and vertebrates. Genetic studies of *C. elegans* sensory cilia have identified a host of factors that are required for their development and maintenance. Many *C. elegans* genes that mutate to cause ciliary defects have human counterparts that mutate to cause ciliopathies (11). Of these, many encode proteins that are associated with the microtubule structure at the heart of the cilium, for example, proteins that modify the microtubule cytoskeleton (12–14). Other mutations affect kinesin- and dynein-dependent transport of cargo into and out of the cilium (i.e., intraflagellar transport) (15). Other genes encode proteins that localize to subcompartments of the cilium and define a complex macromolecular structure within the cilium (16–18).

Some studies have revealed important roles for membrane trafficking systems in ciliary development and maintenance. The machinery for protein synthesis is not present in cilia (19), requiring that ciliary proteins traffic to the cilium from the cell body. The small GTPases Rab8 and Rab11, which function in transport from the trans-Golgi network (TGN) to the plasma membrane, are required for ciliogenesis (20). Mutation of the AP1 clathrin adaptor complex, which mediates the generation of transport vesicles from the Golgi compartment, disrupts localization of odorant receptors to the sensory cilium and is required for normal ciliary structure (21, 22). A component of the kinesin-associated IFT-B particle, IFT20, is enriched on Golgi membranes, suggesting that it might function in the secretory pathway to facilitate transport of cargo destined for the cilium (23). Also, proteins that function in endocytosis are enriched at the base of the sensory cilium, where they might control entry of cargo into the ciliary membrane (22, 24). Mechanisms that select specific proteins early in the secretory pathway for trafficking to the cilium, however, remain poorly understood.

## Significance

**Sensory neurons concentrate the molecular machinery of sensation into a specialized cellular antenna: the cilium. Proteins destined for the cilium are synthesized in the cell body, and poorly understood mechanisms separate them from other cellular proteins and target them to the cilium. Through genetic studies of this process in sensory neurons of the nematode *Caenorhabditis elegans*, we show that a sensory neuron-specific factor that mutates in humans to cause photoreceptor degeneration and blindness regulates an early stage in the trafficking of a key molecule for sensation.**

Author contributions: L.A.M.-V. and N.R. designed research; L.A.M.-V. performed research; L.A.M.-V. contributed new reagents/analytic tools; L.A.M.-V. and N.R. analyzed data; and L.A.M.-V. and N.R. wrote the paper.

The authors declare no conflict of interest.

This article is a PNAS Direct Submission.



[1]To whom correspondence should be addressed. Email: niels.ringstad@med.nyu.edu.

This article contains supporting information online at www.pnas.org/lookup/suppl/doi:10.1073/pnas.1712302115/-/DCSupplemental.



www.pnas.org/cgi/doi/10.1073/pnas.1712302115

To identify factors that function in trafficking to the *C. elegans* sensory cilium, we surveyed genes that (*i*) are highly expressed in *C. elegans* chemosensory BAG neurons, which use a receptor-type guanylate cyclase (rGC) as a chemoreceptor, and (*ii*) are regulated by the DAF-19 transcription factor, which promotes expression of diverse cilium-associated genes (25). This analysis yielded a nematode homolog of the retinopathy gene *Retinal Degeneration 3* (*RD3*). Spontaneous mutations in *RD3* cause early onset photoreceptor degeneration in mice, dogs, and humans (26–28). Photoreceptor cilia of *RD3* mutant mice fail to accumulate guanylate cyclase (29), suggesting that RD3 is required for trafficking of this sensory transduction factor. However, the function of RD3 in membrane trafficking remains unknown and has only been studied in heterologous expression systems. Here, we use in vivo trafficking assays to assign a function for RD3-like factors in regulating exit of rGC cargo from the Golgi and couple these assays to genetic studies that reveal a role for retromer in antagonizing RD3-dependent trafficking.

## Results

**A *C. elegans* Homolog of RD3 Is Required for Sensory Neuron Function.** The cilia of chemosensory BAG neurons are enriched for components of a cGMP-based chemotransduction mechanism (30, 31). Little is known about the molecular factors involved in trafficking these chemotransduction molecules to the sensory cilium. We analyzed a set of 850 genes that are highly expressed in BAG neurons (30) to determine whether any had been identified as potential targets of the RFX family transcription factor DAF-19 (25), which is required for ciliogenesis in many different types of sensory neurons (32) (Fig. 1*A* and Fig. S1). We hypothesized that in addition to genes that encode factors that are constituents of the cilium, the set of DAF-19–regulated genes would include genes that encode factors required for delivery of protein cargo to the sensory cilium. We found 62 genes that were highly expressed in BAG neurons and likely direct targets of DAF-19.

One gene captured by this analysis was a *C. elegans* homolog of a gene that encodes a factor implicated in trafficking to the cilium: *RD3*. RD3 is a small, evolutionarily conserved protein that contains an eponymous structural motif, the RD3 homology domain (RD3HD) (Fig. 1*B*). Interestingly, insects, which do not use cGMP signaling in phototransduction and chemotransduction (33, 34), lack genes that encode RD3-like proteins. Unlike vertebrates, which have at least two *RD3*-like genes, the invertebrate genomes that we examined contain a single *RD3* homolog. Vertebrate *RD3* is preferentially expressed by retinal photoreceptor neurons (29), while the expression pattern of the paralogous *RD3*-like gene has not been studied.

The *C. elegans RD3*-like gene was named *rdl-1*. To determine whether *C. elegans rdl-1* encodes an RD3 homolog that is associated with sensory neurons or whether it is a more broadly expressed paralog, we generated a fosmid-based reporter transgene to determine its cellular expression pattern (35). Expression of *rdl-1::gfp* was restricted to anterior ciliated sensory neurons (Fig. 1*C*). Among the *rdl-1*–expressing neurons are neurons that mediate diverse chemosensory modalities (ASGs, AWBs, AWCs, and BAGs) and AFD thermosensory neurons. These neurons use cGMP-based sensory transduction pathways (36), as do vertebrate photoreceptors, where RD3 is known to be expressed. We used DiI staining (37) to identify two classes of ciliated sensory neuron that are not known to use cGMP signaling in sensory transduction: the ASH and ADL sensory neurons (36, 38–41). We did not detect expression of *rdl-1::gfp* in ASH and ADL neurons (Fig. S2), suggesting that while *rdl-1* is expressed broadly in the sensory nervous system, it is not expressed in all sensory neurons and might not be expressed by sensory neurons that do not use cGMP signaling.

We next tested whether *rdl-1* expression is regulated by DAF-19 as predicted by in silico analysis. We introduced an *rdl-1::gfp* reporter transgene into *daf-19* mutants and measured its expression in two types of ciliated sensory neurons that use rGCs as sensory receptors: chemosensory BAG neurons (31) and thermosensory AFD neurons (42). Expression of *rdl-1::gfp* was significantly decreased by *daf-19* mutation in each of these sensory neuron types (Fig. 1*D*). Together, these data indicate that *rdl-1*, like *RD3*, is specifically expressed by ciliated sensory neurons.

To determine whether *rdl-1* is required for the function of ciliated sensory neurons, we generated *rdl-1* mutants. We used Cas9-mediated mutagenesis to introduce into the *rdl-1* locus frameshifts that are predicted to cause premature stop codons (43) (Fig. 2*A* and Fig. S3*A*). We then assayed the function of *rdl*-1

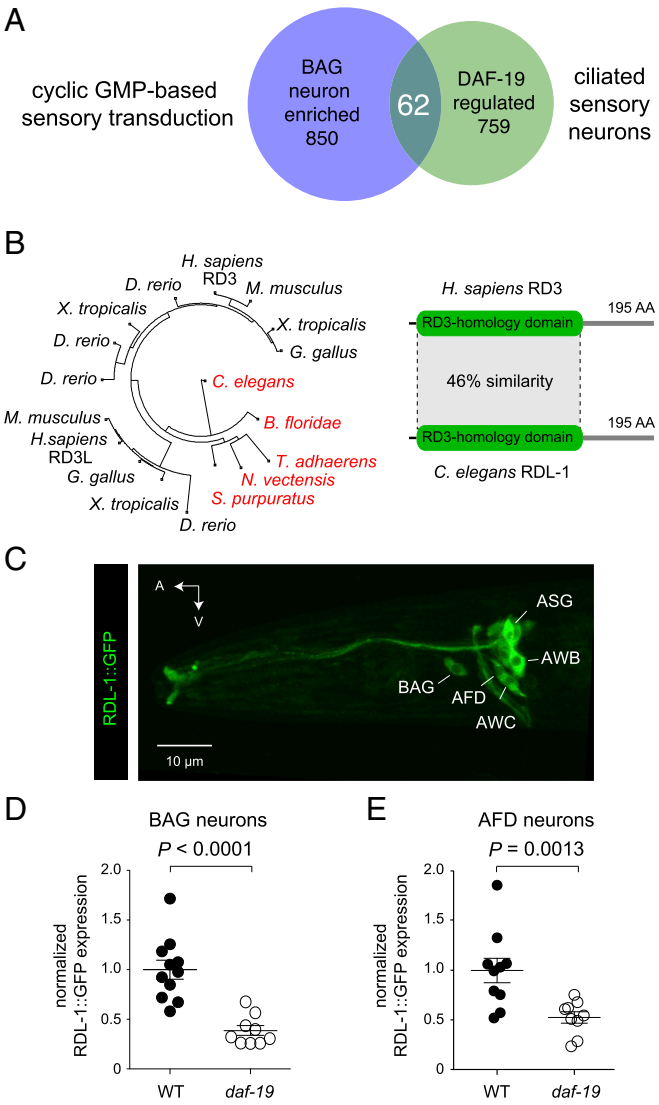


**Fig. 1.** *C. elegans RD3* homolog is a DAF-19 target gene that is expressed in a subset of ciliated sensory neurons. (*A*) Sixty-two genes encode transcripts enriched in BAG-ciliated chemosensory neurons and are predicted targets of the transcription factor DAF-19. (*B*) *rdl-1* encodes the *C. elegans* homolog of vertebrate RD3, a protein that mutates to cause retinal degeneration and is defined by an amino-terminal RD3HD. RD3 homologs from *Branchiostoma floridae*, *Danio rerio*, *Gallus gallus*, *Homo sapiens*, *Mus musculus*, *Nematostella vectensis*, *Strongylocentrotus purpuratus*, *Trichoplax adhaerens*, and *Xenopus tropicalis* were aligned to RDL-1 to generate this dendrogram. AA, amino acids. (*C*) Expression of a fosmid-based *rdl-1::gfp* reporter transgene. A, anterior; V, ventral. (*D* and *E*) Quantification of the effect of *daf-19* mutation on expression of *rdl-1::gfp* in BAG and AFD sensory neurons. *P* was computed using a Mann–Whitney *U* test. WT, wild type.

mutant chemosensory BAG neurons. BAG neurons detect the respiratory gas carbon dioxide ($CO_2$) via a chemotransduction pathway that requires the rGC GCY-9, cyclic nucleotide-gated (CNG) channels comprising TAX-2 and TAX-4 subunits, and L-type calcium channels (30, 31). We tested whether *rdl-1* mutation affects BAG neuron function with a two-choice assay for $CO_2$ avoidance (44, 45). Wild-type animals avoid the sector of the arena with high $CO_2$ levels, while animals defective in BAG neuron function partition equally between the high-$CO_2$ sector and the sector containing room air (Fig. 2*B*). Two independently derived *rdl-1* mutants were significantly defective in $CO_2$ avoidance compared with the wild type. The corresponding mutations failed to complement for this chemotaxis defect, and a transgene expressing RDL-1::GFP fusion restored $CO_2$ avoidance to *rdl-1* mutants (Fig. 2*B*).

We next tested whether *rdl-1* mutation affected BAG neuron physiology by using GCaMP6f (46) to measure calcium responses of wild-type and *rdl-1* mutant BAG neurons to $CO_2$ stimuli. Mutation of *rdl-1* did not affect the morphology of BAG neurons or expression of the GCaMP6f reporter (Fig. S3*B*). The *rdl-1* mutant BAG neurons were partially defective in this calcium response, showing an average peak response to 10% $CO_2$ stimuli that was 30% smaller than the response from wild-type cells (Fig. 2*C*). The distributions of peak responses of wild-type and *rdl-1* mutant cells are shown as cumulative frequency plots, which are simple transformations of histograms in which the fraction of measurements less than or equal to a given value is plotted against that value (Fig. 2*D*). Data from these experiments are also plotted in Fig. S3*C* as a scatter plot. We also noted small but significant differences in the dynamics of the calcium responses of *rdl-1* mutant cells to $CO_2$ stimuli (Fig. S3 *D* and *E*). The *rdl-1* mutant cells took longer to display peak calcium responses (a mean half-time of 2.3 s for mutants compared with 1.6 s for the wild type) and were faster to recover from $CO_2$ stimuli (a mean half-time of 10.8 s for *rdl-1* mutants compared with 14.0 s for the wild type). Together, these behavioral and functional imaging data show that RDL-1 is required for normal function of ciliated sensory neurons that mediate chemotaxis.

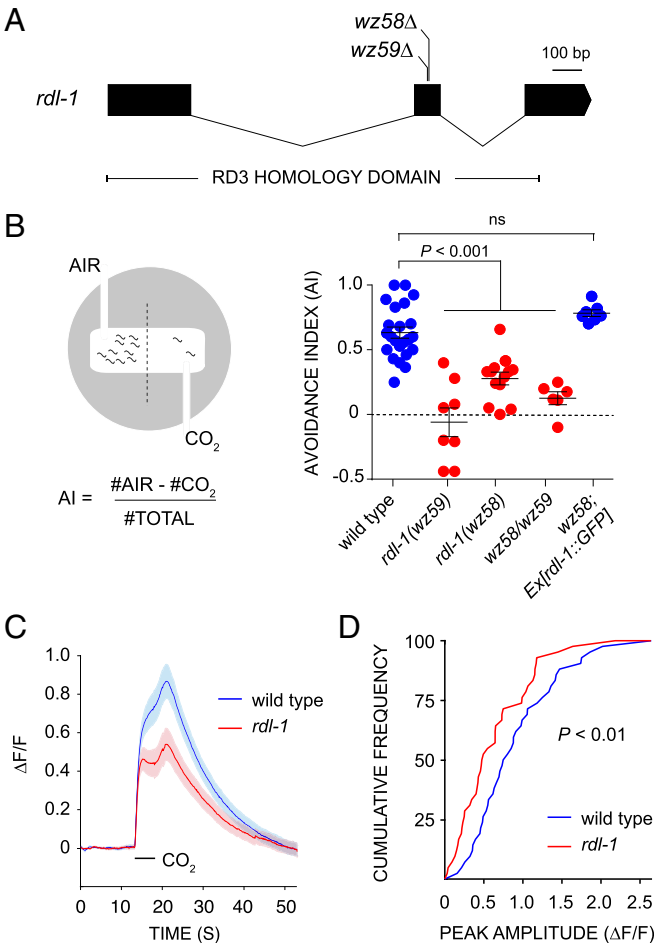


**Fig. 2.** RDL-1 is required for the function of ciliated BAG sensory neurons. (*A*) Gene model for *rdl-1* indicating mutations that were introduced into the second exon by Cas9-mediated mutagenesis. Sequences that encode the RD3HD are underscored. (*B*) Schematic of a $CO_2$-avoidance assay used to test BAG function and definition of the avoidance index (AI) (*Left*). AIs from trials of the wild type, *rdl-1(wz58)*, *rdl-1(wz59)*, *wz58/wz59* transheterozygotes, and *rdl-1(wz58)* mutants expressing RDL-1::GFP fusion (*Right*). Probability was computed using a Mann–Whitney *U* test. ns, not significant. (*C*) Average BAG neuron calcium responses to 10% $CO_2$ are shown. Shaded areas represent the mean ± SEM. Forty-two wild-type and 42 *rdl-1* mutant animals were analyzed. ΔF/F, fractional change in baseline fluorescence. (*D*) Cumulative probability plots for peak ΔF/F values of wild-type and *rdl-1(wz58)* mutant BAG neurons to $CO_2$ stimuli. $P = 0.0096$ according to a Mann–Whitney *U* test.

**RDL-1 Is Required for Trafficking of Receptor-Type Cyclase from the Golgi to the Sensory Cilium.** Because mutation of vertebrate *RD3* causes a defect in localizing rGCs to the photoreceptor outer segment (29), we tested whether its *C. elegans* homolog *rdl-1* has a similar function. We generated animals that express in BAG neurons fluorophore-tagged versions of the rGC GCY-9, the CNG ion channel subunit TAX-4, and the cyclic nucleotide phosphodiesterase PDE-1, which opposes the activity of rGCs in sensory transduction by degrading cGMP and is expressed by BAGs (30, 47) (Fig. 3 *A*–*D*). Mutation of *rdl-1* significantly reduced the fraction of GCY-9 in BAG neuron cilia (Fig. 3*E*). BAG cell-targeted knockdown of *rdl-1* by RNAi caused a similar defect in ciliary cyclase levels, indicating that *rdl-1* functions cell autonomously to promote cyclase localization to the cilium (Fig. S4*A*). By contrast, we did not observe significant effects of *rdl-1* mutation on ciliary localization of TAX-4 CNG channels and the phosphodiesterase PDE-1 (Fig. 3 *F* and *G*).

We next tested whether *rdl-1* was required in a different sensory neuron for enrichment of rGCs in the sensory cilium. GCY-8 is specifically expressed in thermosensory AFD neurons, and is highly enriched in their cilia (17, 48). We found that GCY-8, like GCY-9, required *rdl-1* to be enriched in sensory cilia (Fig. 3*H*). We also tested whether *rdl-1* has a role in trafficking of G protein-coupled (GPCR) odorant receptors to sensory cilia by measuring the effect of *rdl-1* mutation on ciliary enrichment of two odorant receptors native to AWB chemosensory neurons (Fig. 3 *I* and *J*). The *rdl-1* mutation had only a small effect on the ciliary localization of AWB-specific GPCR odorant receptors, although this effect was reproducible and not likely the result of experimental error. Scatter plots of all ciliary localization data are shown in Fig. S4 *B* and *C*.

Next, we tested whether *rdl-1* mutation altered the distribution of rGCs within the BAG sensory cilium. In other sensory neurons, CNG channels cluster in a subcompartment of the ciliary membrane and are separated from guanylate cyclases (17). We found evidence for a similar organization of the BAG sensory cilium. In both wild-type and *rdl-1* mutant BAG cilia, the CNG channel subunit TAX-4 was highly colocalized with the phosphodiesterase PDE-1 in a patch of ciliary membrane. By contrast, the rGC GCY-9 labeled a larger domain of the cilium that included membranes enriched for CNG channels but also included membranes with relatively fewer CNG channels (Fig. 3 *K* and *L* and Fig. S4*D*). Together, these data indicate that RDL-1, like its vertebrate homolog, is required for concentration of rGCs in the sensory cilium. Also, like the outer segments of photoreceptors of vertebrate *RD3* mutants (29), the cilia of *rdl-1* mutant BAG neurons are properly enriched for other sensory transduction molecules, indicating that

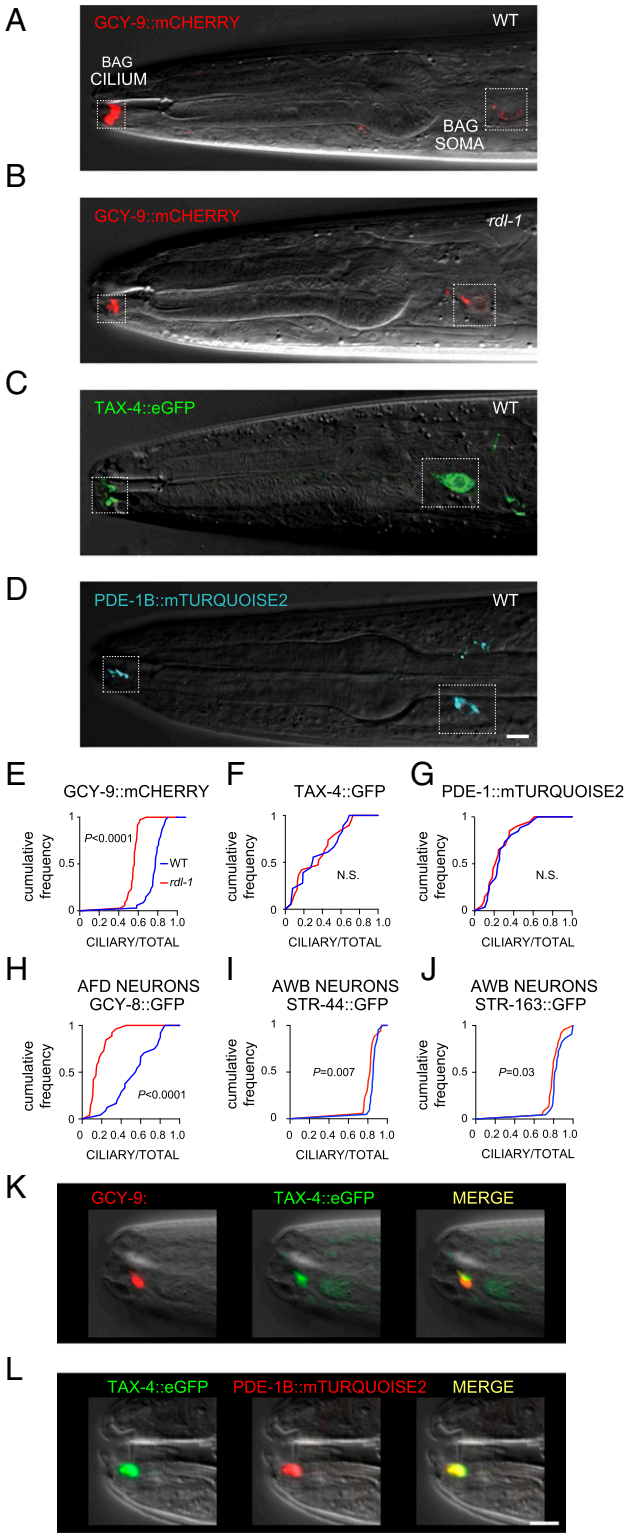


**Fig. 3.** RDL-1 is required for enrichment of rGC in the sensory cilium. (*A* and *B*) Expression of GCY-9::mCherry in wild-type (WT) and *rdl-1* mutant BAG neurons. (*C*) Expression of TAX-4::GFP in BAG neurons. (*D*) Expression of PDE-1B::mTURQUOISE2 in BAG neurons. [Scale bar: 10 μm (also applies to *A*–*C*).] (*E*) Cumulative frequency plot for the enrichment of GCY-9 at the cilium in WT ($n$ = 34) and *rdl-1(wz58)* ($n$ = 35) mutant cells. GCY-9::mCherry in the cilium was normalized to total GCY-9::mCherry (cilium plus soma). (*F*) Cumulative frequency plot for the enrichment of TAX-4 at the cilium in WT ($n$ = 18) and *rdl-1(wz58)* ($n$ = 19) cells. (*G*) Cumulative frequency plot for the enrichment of PDE-1 at the cilium in WT ($n$ = 26) and *rdl-1(wz58)* ($n$ = 20) cells. (*H*) Cumulative frequency plot for enrichment of the rGC GCY-8 in cilia of WT ($n$ = 24) and *rdl-1* ($n$ = 26) thermosensory AFD cells. (*I*) Cumulative frequency plot for enrichment of the GPCR STR-44 in cilia of WT ($n$ = 21) and *rdl-1* ($n$ = 17) AWB neurons. (*J*) Cumulative frequency plot for enrichment of the GPCR STR-163 in cilia of WT ($n$ = 22) and *rdl-1* ($n$ = 23) AWB neurons. (*K* and *L*) Localization of GCY-9, TAX-4, and PDE-1B in BAG cilia. [Scale bar: *L*, 2 μm (also applies to *K*).]

RD3-like factors have a privileged functional connection with rGCs and are dispensable for localization of other ciliary cargo.

Because *rdl-1* is a DAF-19 target gene, many of which are required for cilium formation or maintenance, we examined the structure of sensory cilia in the anterior amphid sensilla using a molecular marker of cilium structure and by transmission electron microscopy. First, we examined the localization of an ARL-13::GFP probe in ciliated sensory neurons. ARL-13 is a small GTPase that is required for ciliogenesis and is highly localized to the cilium proper (49). We observed a normal pattern of ARL-13::GFP enrichment in the cilia of amphidial sensory neurons of *rdl-1* mutants (Fig. 4 *A* and *B*). We next examined the structure of these cilia using electron microscopy. Cilia of amphidial neurons have a highly stereotyped structure (8–10) that is sensitive to mutations that affect intraflagellar transport and microtubule organization. Importantly, *C. elegans* homologs of ciliopathy genes are also required for this stereotyped structure (11). We examined sections of the amphid sensillum in *rdl-1* mutants at positions where ciliary axonemes have stereotyped positions within the amphid, and we observed the expected number and arrangement of ciliary axonemes in *rdl-1* mutants (Fig. 4*B*). At this position, ciliary axonemes also possess a characteristic arrangement of microtubule doublets surrounding microtubule singlets (8–10) (Fig. 4*C*). We noted a small deviation from the expected microtubule arrangements in some amphid cilia of *rdl-1* mutants. Some axonemes in *rdl-1* mutants contained a microtubule doublet that was unraveled (Fig. 4*C*). We observed this defect in the cilia of ASGs and ASIs (two mutants were sectioned and analyzed), but we never observed more than one unraveled doublet per axoneme in these cilia. Cilia of ASEs, which express *rdl-1*, did not display this defect (Fig. 4*C*). We inspected axonemes from four wild-type animals and never observed unraveled doublets, suggesting that this low-penetrance defect is caused by *rdl-1* mutation. However, we did not detect any gross changes in ciliary structure that could explain the defective enrichment of rGCs in sensory cilia of *rdl-1* mutants.

To directly test whether RDL-1 is required for trafficking of the rGC GCY-9 to the BAG neuron cilium, we generated transgenic animals that express a fusion of GCY-9 with the photoconvertible fluorophore mEos3.2 (50) (Fig. 5*A*). We used localized UV irradiation to selectively convert ciliary GCY-9::mEos3.2 from its native green fluorescent state to a red fluorescent state. We then measured the arrival rate of unconverted, green fluorescent GCY-9::mEos3.2 to the cilium (Fig. 5*B*). The *rdl-1* mutants were severely defective in the delivery of GCY-9::mEos3.2 to the sensory cilium (Fig. 5*C*), with an average rate of cyclase delivery that was 24% of the rate observed for the wild type.

Sensory cilia are sites of active membrane and protein turnover. For example, in vertebrate photoreceptors, a large fraction of the outer segment is shed and replenished every day (51). Using the photoconversion assay, we measured the rate at which rGCs in the sensory cilium are removed (Fig. 5*D*). We found that 39% of preexisting rGCs in wild-type BAG neuron cilia were turned over in a 24-h period (Fig. 5*D*), indicating that these cilia are also actively remodeled. We also found that rGC removal from BAG cilia was reduced in *rdl-1* mutants, although the effect was variable and did not reach statistical significance (Fig. 5*E*). A reduced rate of cyclase removal from the cilium might simply be a consequence of reduced rates of incorporation of ciliary rGCs.

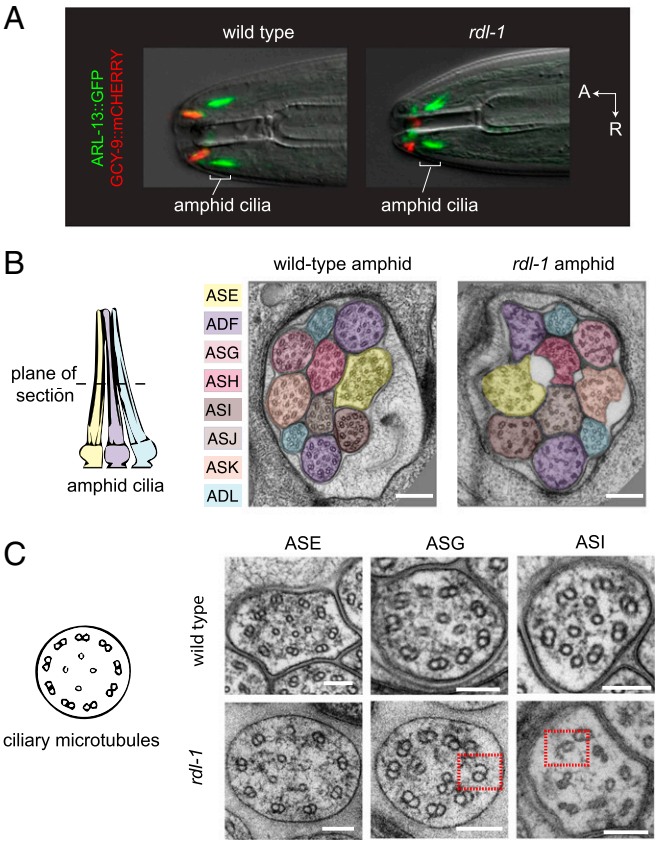


**Fig. 4.** Mutation of *rdl-1* does not grossly alter the structure of sensory cilia. (*A*) ARL-13::GFP enrichment in sensory cilia of the wild type and *rdl-1* mutants. A, anterior; R, right. (Magnification: 750×.) (*B*) Electron micrographs of sections taken through the middle of the amphid ciliary bundle from the wild type and an *rdl-1* mutant. (Scale bars: 200 nm.) (*C*) High-magnification views of wild-type and *rdl-1* mutant axonemes. Unraveled beta-tubules are indicated by red boxes. We examined four wild-type animals and two *rdl-1 (wz58)* mutant animals. (Scale bars: 100 nm.)

To determine whether this difference in cyclase delivery to the cilium could be explained by an effect of *rdl-1* mutation on the rate of rGC synthesis, we designed an experiment in which we photoconverted all visible pools of rGC from green to red and measured the rate of appearance of newly synthesized rGCs (green) (Fig. 5*F*). We did not detect a significant difference in the rates of appearance of newly synthesized rGCs between the two genotypes (Fig. 5*G*), suggesting that loss of RDL-1 affects trafficking of rGCs within the cell.

Next, we examined the dynamics of the pool of rGCs that were in endomembranes in the cell soma. We selectively converted somatic GCY-9::mEos3.2 (Fig. 6*A*) and measured the rate at which newly synthesized (green fluorescent) rGCs accumulated in the cell body (Fig. 6*B*), as well as the extent to which converted (red fluorescent) rGCs were removed (Fig. 6*D*). Nonconverted (green) rGCs accumulated in BAG cell bodies of *rdl-1* mutants to higher levels than they did in the wild type (Fig. 6*C*). This reflected either increased retention of newly synthesized rGCs in the cell body or increased retention of rGCs that had been recycled from the cilium to the soma. In support of the hypothesis that there is increased retention of newly synthesized rGCs in the soma of *rdl-1* mutants, we observed that converted (red) rGCs were retained in the BAG somas of *rdl-1* mutants to a much greater extent than in the wild type (Fig. 6*E*). In sum, our analysis of rGC trafficking in BAG neurons strongly suggests that in vivo RD3-like proteins mediate efficient delivery of rGCs from a somatic pool to the sensory cilium.

To determine the identity of the endomembrane compartment that accumulates rGCs in *rdl-1* mutants, we assayed a panel of

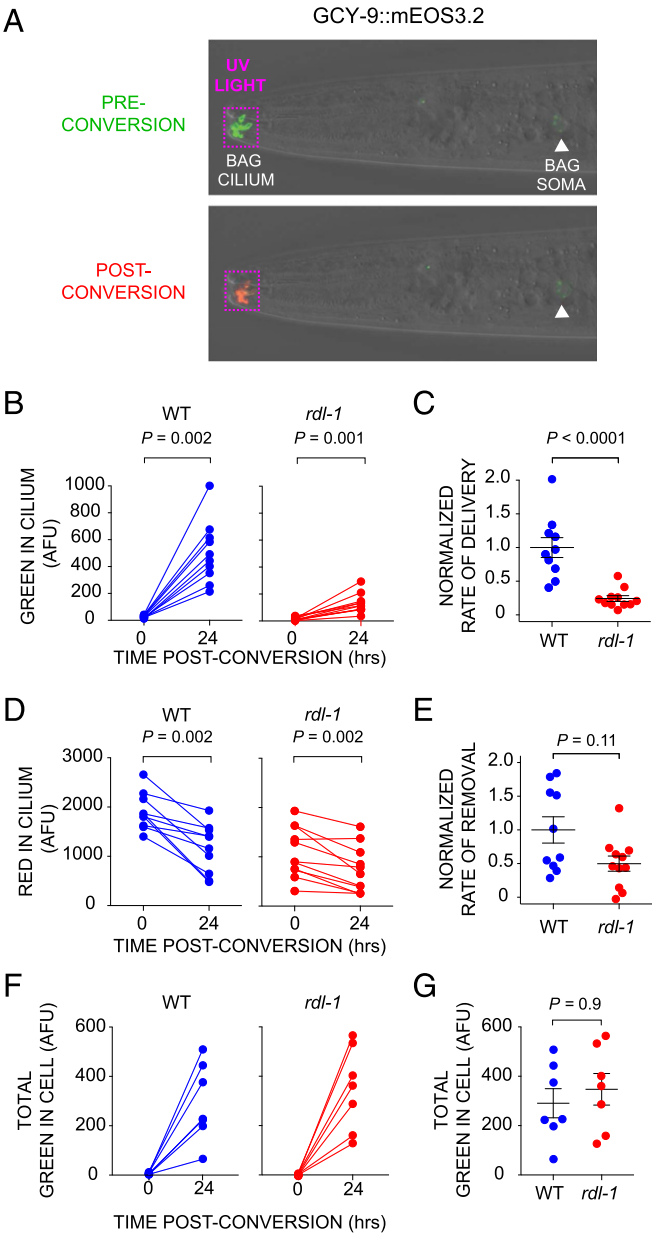


**Fig. 5.** RDL-1 is required for efficient delivery of rGC to the sensory cilium. (*A*) GCY-9::mEos3.2 in BAG neurons before and after photoconversion of GCY-9::mEos3.2 in the sensory cilium. (Magnification: 200×.) (*B*) Measurements of the incorporation of unconverted GCY-9::mEos3.2 into the sensory cilia of wild-type (WT) and *rdl-1(wz58)* mutant BAGs. Before and after plots show paired measurements from the same individual 24 h after photoconversion. (*C*) Rates of incorporation of unconverted (green) GCY-9::mEos3.2 to the sensory cilium of BAG neurons in WT and *rdl-1(wz58)* mutant BAG neurons. (*D*) Measurements of the removal of converted (red) GCY-9::mEos3.2 from the sensory cilia of BAG neurons in WT and *rdl-1(wz58)* mutant BAG cells. (*E*) Rates of removal of converted (red) GCY-9::mEos3.2 from the sensory cilium of BAG neurons in WT and *rdl-1(wz58)* mutant animals. For *B* and *D*, *P* values were calculated with a Wilcoxon two-tailed test. (*F*) Before and after plots of green signal after conversion of all GCY-9::mEos3.2 in the cell. (*G*) Comparison of green fluorescence 24 h post conversion in WT and mutant cells. For *C* and *E*, the measured rates were normalized to the mean rate observed in the WT. *P* values were computed with the Mann–Whitney *U* test. AFU, arbitrary fluorescence units.

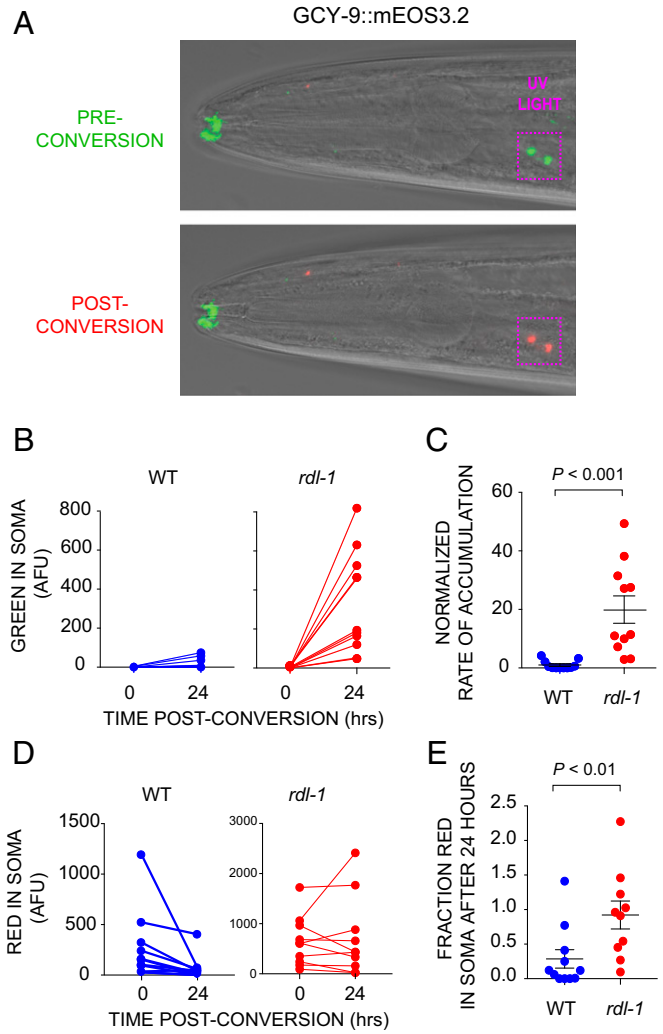


**Fig. 6.** Loss of RDL-1 results in retention of guanylate cyclase in the cell body of BAG neurons. (*A*) GCY-9::mEos3.2 expression in a BAG neuron before (green) and after (red) photoconversion of the pool in somatic endomembranes with a 405-nm laser light. The fluorescence image is overlaid on a differential interface contrast image. (Magnification: 200×.) (*B*) Measurement of the appearance over time of newly synthesized (green in *A*) GCY-9::mEos3.2 in the cell bodies of BAG neurons in the wild-type (WT) and *rdl-1 (wz58)* mutant animals. AFU, arbitrary fluorescence units. (*C*) Rates of accumulation of newly synthesized GCY-9::mEos3.2 (green in *A*) in the soma of BAG neurons in WT and *rdl-1(wz58)* mutants. Rates were normalized to the mean rate of new cyclase appearance measured in the WT. (*D*) Measurements of the amount of converted (red) GCY-9::mEos3.2 retained in BAG neuron somas of the WT and *rdl-1(wz58)* mutants. (*E*) Fraction of converted (red) GCY-9::mEos3.2 remaining in the soma of WT and *rdl-1(wz58)* mutant animals 24 h after photoconversion. For *C* and *E*, *P* values were computed with the Mann–Whitney *U* test. AFU, arbitrary fluorescence units.

transgenic animals expressing fluorescent probes that label endomembrane compartments in BAG neurons. We found that a majority of the GCY-9::mCherry in the soma of *rdl-1* mutants colocalized with the Golgi marker AMAN-2::Venus (52) (Fig. 7*A*). We used the same panel to determine the subcellular localization of an RDL-1::mCherry probe (Fig. S5 *B–D*). RDL-1::mCherry strongly colocalized with the Golgi marker AMAN-2::Venus (Fig. 7*B*). We saw a large majority of RDL-1::mCherry colocalized with AMAN-2::GFP in the BAG cell body, although puncta of RDL-1::mCherry could also be seen in the BAG neuron axon (Fig. S5*A*). Human RD3 and RDL-1 were highly colocalized when expressed in BAG neurons (Fig. 7*D*), suggesting that human RD3 also associates with Golgi membranes in ciliated sensory neurons. Because human and nematode RD3-like proteins display the most sequence similarity in the RD3HD, we hypothesized that

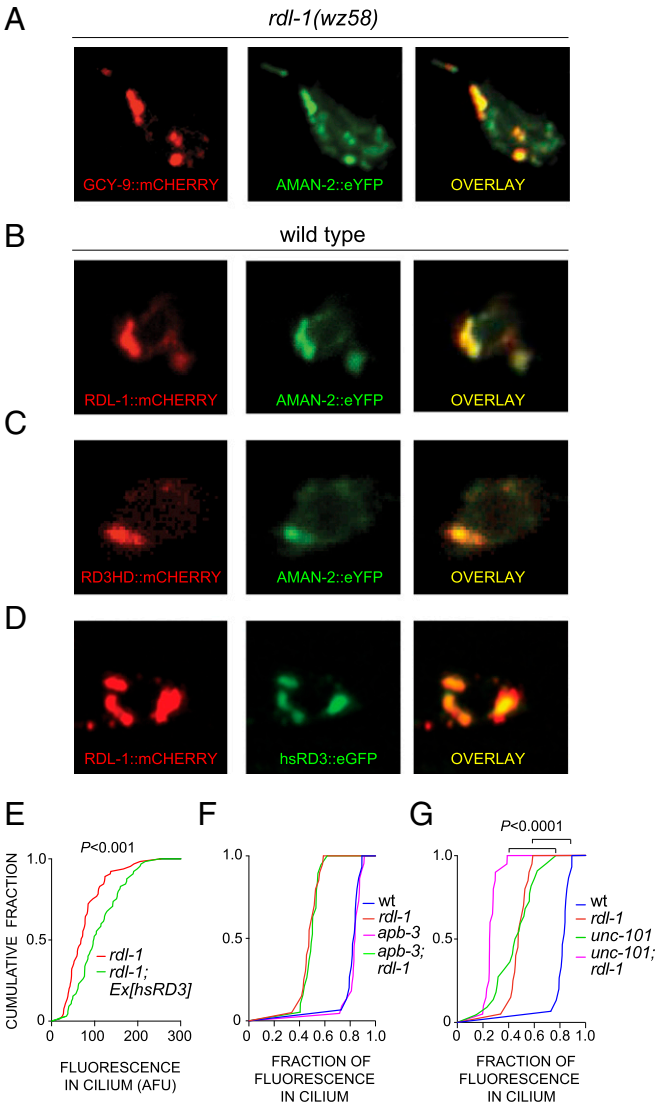


**Fig. 7.** RDL-1 is a Golgi-associated protein that is required for exit of rGC cargo from the Golgi. (*A*) Colocalization of mCherry-tagged GCY-9 (red) with the Golgi marker AMAN-2::Venus (green) in the soma of *rdl-1(wz58)* mutant animals. (*B*) Colocalization of mCherry-tagged RDL-1 (red) with AMAN-2::Venus (green) in the soma of wild-type animals. (*C*) Colocalization of mCherry-tagged RD3HD of *C. elegans* (aa 1–140; red) with AMAN-2::Venus (green) in the soma of wild-type animals. (*D*) Colocalization of mCherry-tagged RDL-1 (red) with GFP-tagged *Homo sapiens* RD3 (green) in the soma of wild-type animals. (*E*) Cumulative fraction of GCY-9::mCherry at the cilium in *rdl-1(wz58)* mutant animals expressing a transgene with the cDNA for *H. sapiens* RD3 in BAG neurons of *rdl-1(wz58)* mutant animals or nontransgenic *rdl-1(wz58)* mutant siblings. Mann–Whitney *U* test, $P = 0.0002$. AFU, arbitrary fluorescence units. (*F*) Cumulative frequency plots of the enrichment of GCY-9 at the cilium in the wild type (wt) and in *rdl-1(wz58), apb-3(ok429),* and *apb-3(ok429); rdl-1(wz58)* mutants. Results of statistical tests for significance: wt vs. *rdl-1*, $P < 0.0001$; wt vs. *apb-3(ok429)*, $P = 0.6862$; wt vs. *apb-3(ok429); rdl-1(wz58)*, $P < 0.0001$; *rdl-1(wz58)* vs. *apb-3(ok429); rdl-1(wz58)*, $P = 0.8754$. (*G*) Cumulative frequency plots for the enrichment of GCY-9 at the cilium in the wt, *rdl-1(wz58)*, *unc-101(m1)*, and *unc-101(m1); rdl-1(wz58)* mutants. The wt and *rdl-1(wz58)* data are replotted from Fig. 6*F*. wt vs. *rdl-1(wz58)*, $P < 0.0001$; wt vs. *unc-101(m1)*, $P < 0.0001$; wt vs. *unc-101(m1); rdl-1(wz58)*, $P < 0.0001$; *rdl-1(wz58)* vs. *unc-101(m1); rdl-1(wz58)*, $P < 0.0001$. For *F* and *G*, *P* values were calculated using the Kolmogorov–Smirnov test. (Magnification: *A–D*, 750×.)

this domain might mediate association to Golgi membranes. Indeed, the RD3HD of RDL-1 was sufficient to associate with Golgi membranes (Fig. 7*C*), indicating that this domain has intrinsic affinity for Golgi membranes in sensory neurons. Finally, because human RD3 colocalized with RDL-1 in BAG neurons, we tested whether it can complement the loss of endogenous RDL-1 and restore rGC delivery to BAG neuron cilia. The *rdl-1* mutants expressing human RD3 had more rGCs in their sensory cilia compared with nontransgenic siblings ($P = 0.0002$, Mann–Whitney *U* test) (Fig. 7*E* and Fig. S6). These data indicate a conserved function of RD3 and RDL-1, and further show that these molecules play a key role in regulating trafficking from the Golgi.

Because our data suggested a role for RDL-1 in regulating post-Golgi transport of rGCs, we next surveyed multiple regulators of post-Golgi transport for their effect on GCY-9 trafficking. AP1 and AP3 clathrin adapters play important roles in sorting cargo from the TGN. In *C. elegans* neurons, AP1 and AP3 function in distinct trafficking pathways. AP3 adapters are required for transport of transmembrane proteins to axons, while AP1 adapters are required for transport of transmembrane proteins to dendritic compartments and to the sensory cilium (21, 22, 53). GCY-9 localization to the sensory cilium was not affected by mutation of the AP3β subunit encoded by *apb-3* (Fig. 7*F* and Fig. S6). Furthermore, *rdl-1; apb-3* double mutants were indistinguishable from *rdl-1* single mutants in this assay (Fig. 7*F* and Fig. S6). By contrast, mutation of *unc-101*, which encodes an AP1μ subunit, caused a significant defect in localization of GCY-9 to the BAG cilium (Fig. 7*G* and Fig. S6). The defect of *unc-101/AP1μ* mutants was comparable to that of *rdl-1* mutants. Analysis of *unc-101; rdl-1* double mutants revealed that the effects of these two mutations are additive (Fig. 7*G* and Fig. S6). These data do not support models in which RDL-1 strictly functions downstream of AP1 adaptors in cyclase trafficking but are consistent with RDL-1 functioning upstream of or in parallel to AP1 adapters. Together, these data show that RDL-1 is a Golgi-associated protein that is required for the efficient exit of rGCs from the Golgi and delivery to the sensory cilium.

**Mutation of Retromer Restores rGC Trafficking to the Sensory Cilium in *rdl-1* Mutants.** After establishing that RDL-1 functions in trafficking from the Golgi to the sensory cilium, we sought to identify membrane trafficking mechanisms that function together with or in antagonism to RDL-1. We performed a targeted genetic screen for mutations that phenocopy or suppress the effects of *rdl-1* mutation. We assembled a panel of viable *C. elegans* mutants for genes that encode proteins required for specific membrane trafficking reactions (Table S1), and tested whether the corresponding mutations either caused defective localization of GCY-9::mCherry or suppressed the defective localization of rGCs in *rdl-1* mutants. We included in this panel a mutant for *daf-25*, which encodes a conserved Myeloid/Nervy/Deaf-1 (MYND) domain-containing protein that is strongly required for trafficking of rGCs, GPCRs, and CNG channel subunits to sensory cilia (16, 17, 54, 55). Strikingly, we found that a mutation in the retromer subunit gene *vps-35* restored GCY-9::mCherry levels in *rdl-1* mutant cilia (Fig. 8 *A–D* and Fig. S7*A*). Retromer is a multisubunit complex that is composed of thee invariant core components (Vps26, Vps29, and Vps35) and variable components that interact with different cargos and membranes (56). We tested whether another core component of retromer encoded by *vps-29* also mutates to suppress the *rdl-1* trafficking defect, and we found that *vps-29* loss of function indeed restored rGC levels to *rdl-1* mutant sensory cilia (Fig. 8*D* and Fig. S7*A*). The *vps-29* and *vps-35* single mutants each had elevated levels of GCY-9::mCherry in BAG neuron cilia, indicating that retromer normally functions in sensory neurons to limit the amount of rGC cargo that is sent to the cilium (Fig. 8*E* and Fig. S7*B*). We expressed VPS-35::YFP fusion together with RDL-1::mCherry in BAG neurons and observed little colocalization

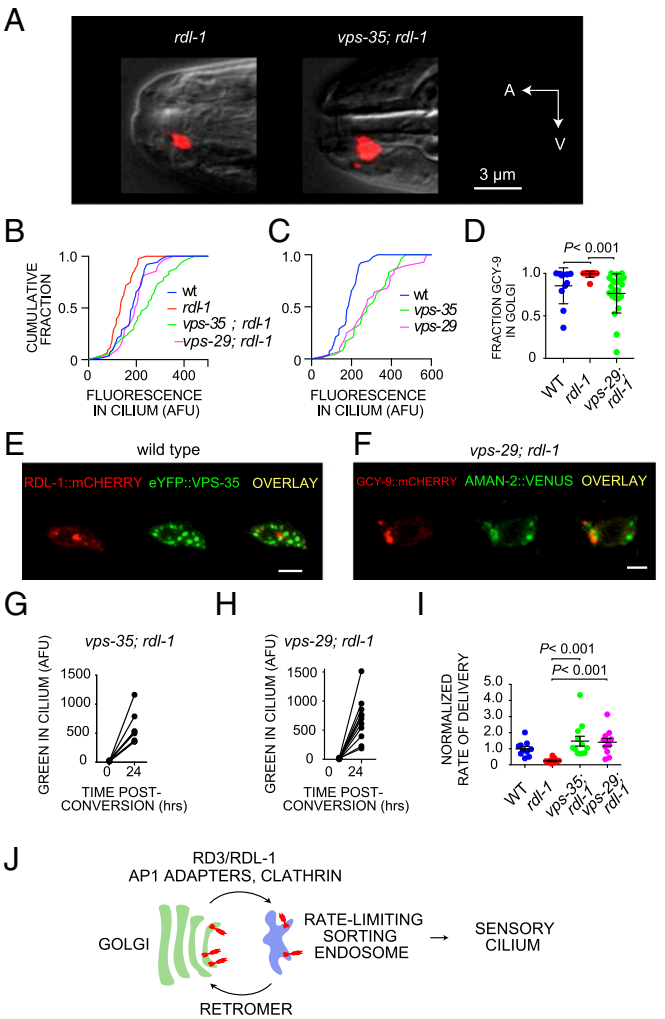


**Fig. 8.** Mutations in components of the retromer complex increase delivery to the sensory cilium in *rdl-1* mutant animals. (*A*) BAG cilia in *rdl-1* mutants and in *vps-35; rdl-1* double mutants labeled with GCY-9::mCherry. A, anterior; V, ventral. (*B*) Cumulative frequency plot for the enrichment of GCY-9 at the cilium in the wild type (wt or WT), *rdl-1(wz58), vps-35(ep442); rdl-1(wz58); vps-35(ok1880); rdl-1(wz58), and vps-29(tm1320); rdl-1(wz58)* mutant animals. Results of Kolmogorov–Smirnov statistical tests for significance: wt ($n = 52$) vs. *rdl-1(wz58)* ($n = 43$), $P = 0.0006$; *rdl-1(wz58)* vs. *vps-35(ep442); rdl-1(wz58)* ($n = 34$), $P < 0.0001$; *rdl-1(wz58)* vs. *vps-29(tm1320); rdl-1(wz58)* ($n = 28$), $P = 0.002$. (*C*) Cumulative frequency plot for levels of enrichment of GCY-9 at the cilium in the wt and in *vps-35(ep442)* and *vps-29(tm1320)* mutants. Results of Kolmogorov–Smirnov statistical tests for significance: wt vs. *vps-35(ep442)* ($n = 24$), $P < 0.0001$; wt vs. *vps-29(tm1320)* ($n = 28$), $P < 0.0001$. Data for the wt are replotted from *B*. (*D*) Quantification of the fraction of mCherry-tagged GCY-9 colocalized with AMAN-2 in the WT ($n = 11$), *rdl-1(wz58)* ($n = 13$), *and vps-29 (tm1320); rdl-1(wz58)* mutants ($n = 22$). Results of Mann–Whitney *U* statistical tests for significance: WT vs. *rdl-1(wz58)*, $P = 0.0003$; *rdl-1(wz58)* vs. *vps-29 (tm1320); rdl-1(wz58)*, $P < 0.0001$;WT vs. *vps-29(tm1320); rdl-1(wz58)*, $P = 0.1432$. (*E*) mCherry-tagged RDL-1 (red) colocalization with enhanced yellow fluorescent protein (eYFP)-tagged VPS-35 (green). (*F*) GCY-9::mCherry (red) colocalization with VENUS-tagged AMAN-2 (green) in *vps-29(tm1320); rdl-1 (wz58)* mutants. (Scale bars: *E* and *F*, 2 μm.) (*G*) Incorporation of unconverted GCY-9 into the sensory cilia of *vps-35(ep442); rdl-1(wz58)* mutant BAGs ($n = 12$). Before and after plots show paired measurements from the same individual. (*H*) Incorporation of unconverted GCY-9 into the sensory cilia of *vps-29 (tm1320); rdl-1(wz58)* mutant BAGs ($n = 10$). (*I*) Rates of incorporation of unconverted (green) GCY-9::mEos3.2 to the sensory cilium of BAG neurons in WT, *rdl-1(wz58), vps-29(tm1320); rdl-1(wz58)*, and *vps-35(ep442); rdl-1(wz58)* mutant BAG neurons. The data for WT and *rdl-1(wz58)* have been replotted from Fig. 4*C*. *P* values were calculated using the Mann–Whitney *U* test. (*J*) Model for the roles of RDL-1, AP1 adapters, and clathrin, and for the retromer complex in rGC trafficking to the cilium. AFU, arbitrary fluorescence units.

of these two reporters (Fig. 8*G*), suggesting that retromer and RD3-like factors function on different endomembrane compartments to regulate rGC trafficking.

Because retromer mediates egress of cargo from endosomes for retrograde endosome-to-Golgi trafficking, we hypothesized that retromer mutation would cause cargo to accumulate in a post-Golgi endomembrane. We examined the localization of GCY-9::mCherry in double mutants for *rdl-1* and retromer. In *rdl-1* single mutants, almost all GCY-9::mCherry was colocalized with AMAN-2::Venus in the Golgi (Figs. 7*A* and 8*F*). Mutation of *vps-29* in *rdl-1* mutants disrupted this colocalization and shifted a significant fraction of GCY-9::mCherry to a non-Golgi endomembrane compartment in BAG neurons (Fig. 8 *C* and *F*). In some cases, we also observed that mutation of *vps-29* partially changed the distribution of the AMAN-2::Venus probe within BAG neurons; in addition to large puncta of AMAN-2::Venus, *vps-29* mutants displayed perinuclear AMAN-2::Venus (Fig. S7*C*). This might reflect a change in Golgi morphology caused by retromer mutation, or it might indicate partial mislocalization of the AMAN-2::Venus probe to a non-Golgi compartment. We note that if some AMAN-2::Venus probe were mislocalized to non-Golgi compartments in retromer mutants, this would introduce a bias in favor of observing colocalization of AMAN-2 and rGCs. We observed the opposite. These data indicate that in double mutants for a retromer component and *rdl-1*, the restoration of delivery of rGCs to sensory cilia correlates with the accumulation of rGCs in a non-Golgi compartment that is likely an endosome. We tested whether mutation of retromer causes rGC cargo to colocalize with RAB-5 in early endosomes or with either RAB-8 or RAB-11, which marks endosomes previously linked to trafficking of GPCRs to the cilium (22, 57–62). We could not detect colocalization of any of these RABs with GCY-9::mCherry cargo (Fig. S6), suggesting that the endomembrane compartment in which rGC cargo accumulates has a molecular composition distinct from endosomes that are linked to GPCR trafficking.

To demonstrate that suppression of *rdl-1* by retromer mutation is caused by restoration of trafficking, we directly measured the effect of retromer mutation on the rate of delivery of rGCs to the cilium in *rdl-1* mutants using GCY-9::mEos3.2 (Fig. 8 *G–I*). Mutation of *vps-35* and *vps-29* each restored the rate of delivery of unconverted GCY-9::mEos3.2 to wild-type levels (Fig. 8*I*). These data indicate that retromer mutation suppressed the *rdl-1* defect by restoring rGC trafficking from the soma to the cilium.

## Discussion

**Retromer Antagonizes Delivery of rGC Cargo to the Sensory Cilium.** Our data indicate that RD3-like factors play a critical and previously unappreciated role in releasing cargo destined for the sensory cilium from the Golgi compartment. Loss of RDL-1, the sole RD3 homolog of *C. elegans*, caused a decrease in the delivery of rGC to the sensory cilium and a concomitant retention of cyclase in the Golgi. Strikingly, delivery of rGCs to the cilium could be restored by mutating retromer. In *C. elegans*-ciliated sensory neurons, retromer is principally associated with endosomal membranes. Together, these data support a model in which the rate of delivery of rGCs to the cilium is determined by how much cargo accumulates in an endosomal compartment from which it is sorted to the cilium (Fig. 8*J*). According to this model, steady-state levels of cargo at the endosome are determined by the rate of delivery of cargo to endosomes, which is RD3-dependent, and by the rate of its removal from the endosome, which is mediated by retromer. Because loss of RDL-1 does not completely eliminate post-Golgi trafficking of rGCs, concentrations of rGCs in a sorting endosome are restored by slowing their egress. In support of this model, we observed accumulation of rGC cargo in non-Golgi endosomal membranes when we mutated retromer, and we propose that this compartment is the next stage in rGC trafficking to the cilium.

That loss of retromer ameliorates the cellular phenotype of *C. elegans* sensory neurons lacking the RD3 homolog suggests that retromer might be a therapeutic target for the treatment of disorders caused by an underlying defect in trafficking to the cilium. For example, *Rd3* is one of more than 238 genes that mutate to cause degeneration of retinal photoreceptor neurons (5). It is possible that some of these genes encode factors that, like RD3, are required for trafficking to the cilium through mechanisms that are antagonized by retromer. Because of its established role in regulating exit from the endosome, retromer is already considered a promising therapeutic target for treatment for neurodegenerative disorders caused by pathological protein aggregates (63). Compounds that stabilize active retromer complexes accelerate the clearance of APP from the endosome before it can be cleaved (64). Through this mechanism, retromer agonists might delay or even halt the progression of pathophysiology caused by toxic protein aggregates in neurons. Our study of interactions between retromer-dependent trafficking and a nematode homolog of a retinopathy gene illustrates how retromer antagonists might have therapeutic value in pathological states caused by dysfunction of intracellular trafficking mechanisms. A similar beneficial effect of retromer mutation was observed in studies of glial morphogenesis, in which retromer mutation restored glial morphology to *daf-6* mutants, which lack a Patched-related protein (65). In this study, specific sorting nexins (SNX-1 and SNX-3) were implicated in antagonizing DAF-6 function. By contrast, we found no role for SNX-1 and SNX-3 in regulating rGC trafficking (Table S1), indicating distinct functions for different retromer complexes. These observations motivate efforts to identify sorting nexins or adaptors that recruit rGCs and other cargo for retrograde transport from the endosome to the TGN. Pharmacological agents that dissociate specific cargo from their adaptors might be useful therapeutic targets for the treatment of a subset of disorders caused by defective trafficking of proteins to cilia or other cellular destinations.

**RD3-Like Proteins Confer a Molecular Specialization to the Golgi in Ciliated Sensory Neurons.** A remarkable feature of RD3/RDL-1–mediated trafficking is its specificity for a subset of ciliary cargo. In vertebrate and nematode sensory neurons, rGC trafficking requires RD3/RDL-1, but other cargo, such as CNG channel subunits and cGMP phosphodiesterase, does not (29). We also only measured a small effect of loss of RDL-1 on trafficking of GPCRs to the sensory cilium of AWB neurons. Why might different components of a sensory transduction pathway use different mechanisms for delivery to the sensory cilium? One possibility is that sensory transduction factors must be replenished at different rates. Indeed, our data reveal that rGCs in *C. elegans* sensory cilia turn over at a remarkably high rate; ~40% of the rGC content of BAG cell cilia is removed every 24 h. This turnover might suggest a process in BAG neurons that is similar to the constitutive remodeling of photoreceptor outer segments, which are shed and then regenerate daily (5). We have not directly observed such shedding events, however, and it is also possible that cyclase turnover reflects an endocytic process that returns ciliary cyclase to the cell body. Whether or not nematode rGCs are shed through an analogous mechanism, it might be that these molecules are unusually labile in both vertebrate and nematode sensory neurons, and, consequently, must be synthesized and trafficked at a different rate than other constituents of the sensory cilium. It is also possible, however, that there is no property of rGCs that distinguishes them from other ciliary constituents. During evolution, sensory cilia might have acquired in a piecemeal manner the ability to recruit different signaling factors, and the conserved role for RD3-like factors in cyclase trafficking might simply reflect this evolutionary history.

Whatever its origins, a comparison of vertebrate and nematode rGCs and RD3-like factors suggests that the functional relationship between these factors is linked to ciliary function and not to rGCs per se. Unlike vertebrate cells, most nematode cells lack a

primary cilium, with ciliated sensory neurons being the exception. Many nematode rGCs, however, are expressed outside of the sensory nervous system, for example, in nonsensory neurons and in nonneural tissues (66). We found no evidence that the sole RD3-like factor of *C. elegans*, RDL-1, was expressed in nonciliated cells that express rGCs, suggesting that RDL-1 facilitation of rGC trafficking is especially critical in ciliated neurons. In vertebrates, expression of RD3 is restricted to retinal photoreceptor neurons, but there is also a second vertebrate gene that encodes an RD3 paralog, whose expression pattern has not been well characterized. It is possible that this RD3-like factor promotes sorting of rGCs or other signaling factors to nonsensory cilia. It will be interesting to determine whether this RD3 paralog also functions in trafficking from the Golgi.

Our study, together with studies of vertebrate RD3, indicates that in ciliated sensory neurons, rGC cargo is differentiated from other proteins at an early stage of the secretory pathway, at the latest, by the time it exits the Golgi. Based on studies of rGC trafficking in a heterologous expression system, there is evidence that RD3 can also function to promote exit of rGCs from the endoplasmic reticulum (29). These studies suggest that rGC trafficking might be differentiated from the trafficking of other cargo even before rGCs enter the Golgi. Our data, however, indicate that the exit of rGCs from the Golgi in ciliated sensory neurons is especially sensitive to loss of an RD3-like factor. Two lines of evidence support the conclusion that ciliary cargoes are already segregated at this early stage in the secretory pathway. First, in *C. elegans* sensory neurons, other proteins destined for the sensory cilium do not require the Golgi-associated RD3-like factor RDL-1 for trafficking. Second, GPCR odorant receptors stringently require Golgi-associated AP1 adapters for trafficking to the cilium (21, 22), whereas we found that rGCs still traffic to the sensory cilia of *unc-101* mutants, although that trafficking is reduced. There is no self-evident a priori reason for ciliary proteins to be segregated from other cargo in the secretory pathway of sensory neurons, making the existence of such a specialization especially intriguing.

The existence of multiple trafficking pathways to the cilium associated with distinct cargo creates a remarkable potential for structural and functional plasticity of this organelle. The morphology of *C. elegans* sensory cilia is affected by sensory neuron activity and by changes in the internal milieu. Mutants defective in chemotransduction and thermotransduction display alterations in ciliary morphology (48, 67). Other mutants have defective ciliary morphology because the extracellular environment generated by support cells that surround sensory nerve endings has been altered (48, 68, 69). Environment and experience therefore influence the shape and size of sensory cilia. Because delivery of different ciliary proteins to sensory endings is mediated by multiple mechanisms, sensory neurons might be able to rapidly and flexibly alter the molecular composition of sensory cilia. As more molecules required for trafficking to the sensory cilium are characterized, it will be possible to test this conjecture and determine whether the distributed mechanisms that route proteins to the cilium are not only required to generate and maintain the cilium but also serve to remodel this signaling compartment and alter its functional properties.

## Materials and Methods

Extended materials and methods are found in *SI Materials and Methods*.

***C. elegans* Strains Used in This Study.** Strains used in this study are listed in Table S2 in the order in which they appear. Plasmids used to generate transgenic animals are listed in Table S3. The *rdl-1* mutants were generated by CAS9-mediated mutagenesis (43). Transgenic *C. elegans* was generated using standard procedures (70). In some cases, extrachromosomal transgenes were integrated by gamma-irradiation (5,000 rads). Strains were grown on 6-cm nematode growth medium (NGM) agar plates at 20 °C or 25 °C on *Escherichia coli* OP50 as described (71).

**$CO_2$-Avoidance Assays.** A total of 20–30 adult hermaphrodites were placed on an unseeded 10-cm NGM plate. A custom-made chamber was pressed into the NGM media, trapping the animals in the chamber. Gas mixes were introduced at 1.5 mL·min$^{-1}$ using a syringe pump (New Era, Inc.). After 30 min, animals were scored as being either on the side with the $CO_2$ inlet or on the side with the air inlet.

**Microscopy and Image Analysis.** Animals were mounted on a 2% agarose pad containing either 30 mM sodium azide or 10 mM levamisole hydrochloride. Fluorescence and differential interface contrast micrographs were acquired using an LSM700 laser-scanning confocal microscope (Zeiss) using a 40× objective (1.4 N.A.). Z-projections of image stacks were generated with ImageJ (NIH) (72). Quantitation of fluorescence signals and colocalization analysis were also performed using ImageJ.

**In Vivo Calcium Imaging.** In vivo calcium imaging was performed as previously described (31). For analysis of calcium signals in BAG neurons, an ImageJ macro computed background as the mean of the 30 dimmest pixels in an image and the signal as the mean of the 15 brightest pixels within a region of interest that contained the cell body. Signal and background measurements were analyzed using MATLAB (MathWorks) scripts that corrected for linear baseline drift and determined peak responses and rise and decay times for each cellular response.

**Transmission Electron Microscopy.** Young adult *C. elegans* was processed for high-pressure freezing using 20% BSA as a mounting medium. Freeze substitution was performed with a Leica EM AFS2 system. Samples were embedded in EMbed 812 (Electron Microscopy Sciences). Serial ultrathin sections (70 nm) were cut, mounted on 2 × 1-mm copper slot grids, and stained with uranyl acetate and lead citrate. Sections were imaged with a Philips CM-12 electron microscope (FEI) and photographed with a Gatan (4k × 2.7k) digital camera (Gatan, Inc.). Five wild-type and two *rdl-1(wz58)* mutant animals were sectioned and imaged.

**mEos3.2 Photoconversion Assays.** mEos3.2 photoconversion and image acquisition were performed on an LSM700 laser-scanning confocal microscope using a 40× objective (1.4 N.A.). Animals were immobilized with 30 mM sodium azide, and a 405-nm laser was used to convert mEos3.2. Animals were recovered with a drop of M9, transferred to seeded 6-cm NGM plates, and reimaged after 24 h.

**Statistical Analysis.** GraphPad Prism was used to perform statistical tests.

**ACKNOWLEDGMENTS.** Alice Liang, Chris Petzold, and Kristen Dancel-Manning acquired transmission electron microscopy images for this study. Michael Cammer wrote ImageJ macros that were used for analysis of calcium imaging data. We thank the N.R. laboratory and Jeremy Nance for helpful comments, and Malan Silva for bringing the ciliary defect of *rdl-1* mutants to our attention. Maureen Barr (Rutgers University), Ken Miller (Oklahoma Medical Research Foundation), Piali Sengupta (Brandeis University), and Shai Shaham and Aakanshka Singhvi (Rockefeller University) provided plasmids and strains used in this study. We also received mutant strains from Shohei Mitani (Tokyo Women's Medical University) and from the Caenorhabditis Genetics Center (University of Minnesota), which was funded by NIH Office of Research Infrastructure Programs Grant P40 OD010440. This research was supported by NIH Grant R35 GM122573. L.A.M.-V. received support from Training Grants T32GM007308 and T32NS086750 as well as National Research Service Award Fellowship NEI F31EY024836.

1. Kim S, Dynlacht BD (2013) Assembling a primary cilium. *Curr Opin Cell Biol* 25:506–511.
2. Fliegauf M, Benzing T, Omran H (2007) When cilia go bad: Cilia defects and ciliopathies. *Nat Rev Mol Cell Biol* 8:880–893.
3. Singla V, Reiter JF (2006) The primary cilium as the cell's antenna: Signaling at a sensory organelle. *Science* 313:629–633.
4. Pifferi S, Menini A, Kurahashi T (2010) Signal transduction in vertebrate olfactory cilia. *The Neurobiology of Olfaction*, Frontiers in Neuroscience, ed Menini A (CRC Press, Boca Raton, FL).
5. Molday RS, Moritz OL (2015) Photoreceptors at a glance. *J Cell Sci* 128:4039–4045.
6. Inglis PN, Ou G, Leroux MR, Scholey JM (2007) The sensory cilia of Caenorhabditis elegans. *WormBook*, 10.1895/wormbook.1.126.2.
7. Perkins LA, Hedgecock EM, Thomson JN, Culotti JG (1986) Mutant sensory cilia in the nematode Caenorhabditis elegans. *Dev Biol* 117:456–487.
8. Ward S, Thomson N, White JG, Brenner S (1975) Electron microscopical reconstruction of the anterior sensory anatomy of the nematode Caenorhabditis elegans. *J Comp Neurol* 160:313–337.
9. Ware RW, Clark D, Crossland K, Russell RL (1975) The nerve ring of the nematode Caenorhabditis elegans: Sensory input and motor output. *J Comp Neurol* 162:71–110.

10. Doroquez DB, Berciu C, Anderson JR, Sengupta P, Nicastro D (2014) A high-resolution morphological and ultrastructural map of anterior sensory cilia and glia in Caenorhabditis elegans. *eLife* 3:e01948.
11. Bae YK, Barr MM (2008) Sensory roles of neuronal cilia: Cilia development, morphogenesis, and function in C. elegans. *Front Biosci* 13:5959–5974.
12. O'Hagan R, et al. (2011) The tubulin deglutamylase CCPP-1 regulates the function and stability of sensory cilia in C. elegans. *Curr Biol* 21:1685–1694.
13. Shida T, Cueva JG, Xu Z, Goodman MB, Nachury MV (2010) The major alpha-tubulin K40 acetyltransferase alphaTAT1 promotes rapid ciliogenesis and efficient mechanosensation. *Proc Natl Acad Sci USA* 107:21517–21522.
14. Janke C, Kneussel M (2010) Tubulin post-translational modifications: Encoding functions on the neuronal microtubule cytoskeleton. *Trends Neurosci* 33:362–372.
15. Prevo B, Scholey JM, Peterman EJG (2017) Intraflagellar transport: Mechanisms of motor action, cooperation, and cargo delivery. *FEBS J* 284:2905–2931.
16. Wojtyniak M, Brear AG, O'Halloran DM, Sengupta P (2013) Cell- and subunit-specific mechanisms of CNG channel ciliary trafficking and localization in C. elegans. *J Cell Sci* 126:4381–4395.
17. Nguyen PA, Liou W, Hall DH, Leroux MR (2014) Ciliopathy proteins establish a bipartite signaling compartment in a C. elegans thermosensory neuron. *J Cell Sci* 127: 5317–5330.
18. Blacque OE, Sanders AA (2014) Compartments within a compartment: What C. elegans can tell us about ciliary subdomain composition, biogenesis, function, and disease. *Organogenesis* 10:126–137.
19. Pazour GJ, Bloodgood RA (2008) Targeting proteins to the ciliary membrane. *Curr Top Dev Biol* 85:115–149.
20. Das A, Guo W (2011) Rabs and the exocyst in ciliogenesis, tubulogenesis and beyond. *Trends Cell Biol* 21:383–386.
21. Dwyer ND, Adler CE, Crump JG, L'Etoile ND, Bargmann CI (2001) Polarized dendritic transport and the AP-1 mu1 clathrin adaptor UNC-101 localize odorant receptors to olfactory cilia. *Neuron* 31:277–287.
22. Kaplan OI, et al. (2010) The AP-1 clathrin adaptor facilitates cilium formation and functions with RAB-8 in C. elegans ciliary membrane transport. *J Cell Sci* 123: 3966–3977.
23. Follit JA, Tuft RA, Fogarty KE, Pazour GJ (2006) The intraflagellar transport protein IFT20 is associated with the Golgi complex and is required for cilia assembly. *Mol Biol Cell* 17:3781–3792.
24. Kaplan OI, et al. (2012) Endocytosis genes facilitate protein and membrane transport in C. elegans sensory cilia. *Curr Biol* 22:451–460.
25. Efimenko E, et al. (2005) Analysis of xbx genes in C. elegans. *Development* 132: 1923–1934.
26. Friedman JS, et al. (2006) Premature truncation of a novel protein, RD3, exhibiting subnuclear localization is associated with retinal degeneration. *Am J Hum Genet* 79: 1059–1070.
27. Chang B, Heckenlively JR, Hawes NL, Roderick TH (1993) New mouse primary retinal degeneration (rd-3). *Genomics* 16:45–49.
28. Kukekova AV, et al. (2009) Canine RD3 mutation establishes rod-cone dysplasia type 2 (rcd2) as ortholog of human and murine rd3. *Mamm Genome* 20:109–123.
29. Azadi S, Molday LL, Molday RS (2010) RD3, the protein associated with Leber congenital amaurosis type 12, is required for guanylate cyclase trafficking in photoreceptor cells. *Proc Natl Acad Sci USA* 107:21158–21163.
30. Hallem EA, et al. (2011) Receptor-type guanylate cyclase is required for carbon dioxide sensation by Caenorhabditis elegans. *Proc Natl Acad Sci USA* 108:254–259.
31. Smith ES, Martinez-Velazquez L, Ringstad N (2013) A chemoreceptor that detects molecular carbon dioxide. *J Biol Chem* 288:37071–37081.
32. Swoboda P, Adler HT, Thomas JH (2000) The RFX-type transcription factor DAF-19 regulates sensory neuron cilium formation in C. elegans. *Mol Cell* 5:411–421.
33. Hardie RC, Juusola M (2015) Phototransduction in Drosophila. *Curr Opin Neurobiol* 34:37–45.
34. Vosshall LB, Stocker RF (2007) Molecular architecture of smell and taste in Drosophila. *Annu Rev Neurosci* 30:505–533.
35. Tursun B, Cochella L, Carrera I, Hobert O (2009) A toolkit and robust pipeline for the generation of fosmid-based reporter genes in C. elegans. *PLoS One* 4:e4625.
36. Komatsu H, Mori I, Rhee JS, Akaike N, Ohshima Y (1996) Mutations in a cyclic nucleotide-gated channel lead to abnormal thermosensation and chemosensation in C. elegans. *Neuron* 17:707–718.
37. Starich TA, et al. (1995) Mutations affecting the chemosensory neurons of Caenorhabditis elegans. *Genetics* 139:171–188.
38. Ortiz CO, et al. (2009) Lateralized gustatory behavior of C. elegans is controlled by specific receptor-type guanylyl cyclases. *Curr Biol* 19:996–1004.
39. Yu S, Avery L, Baude E, Garbers DL (1997) Guanylyl cyclase expression in specific sensory neurons: A new family of chemosensory receptors. *Proc Natl Acad Sci USA* 94: 3384–3387.
40. Krzyzanowski MC, et al. (2016) Aversive behavior in the nematode C. elegans is modulated by cGMP and a neuronal gap junction network. *PLoS Genet* 12:e1006153.
41. Bargmann CI (2006) Chemosensation in C. elegans. *WormBook*, 10.1895/wormbook.1.123.1.
42. Takeishi A, et al. (2016) Receptor-type guanylyl cyclases confer thermosensory responses in C. elegans. *Neuron* 90:235–244.
43. Friedland AE, et al. (2013) Heritable genome editing in C. elegans via a CRISPR-Cas9 system. *Nat Methods* 10:741–743.
44. Brandt JP, Ringstad N (2015) Toll-like receptor signaling promotes development and function of sensory neurons required for a C. elegans pathogen-avoidance behavior. *Curr Biol* 25:2228–2237.
45. Carrillo MA, Guillermin ML, Rengarajan S, Okubo RP, Hallem EA (2013) O2-sensing neurons control CO2 response in C. elegans. *J Neurosci* 33:9675–9683.
46. Chen TW, et al. (2013) Ultrasensitive fluorescent proteins for imaging neuronal activity. *Nature* 499:295–300.
47. Rojo Romanos T, Petersen JG, Pocock R (2017) Control of neuropeptide expression by parallel activity-dependent pathways in Caenorhabditis elegans. *Sci Rep* 7:38734.
48. Singhvi A, et al. (2016) A glial K/Cl transporter controls neuronal receptive ending shape by chloride inhibition of an rGC. *Cell* 165:936–948.
49. Warburton-Pitt SR, Silva M, Nguyen KC, Hall DH, Barr MM (2014) The nphp-2 and arl-13 genetic modules interact to regulate ciliogenesis and ciliary microtubule patterning in C. elegans. *PLoS Genet* 10:e1004866.
50. Zhang M, et al. (2012) Rational design of true monomeric and bright photoactivatable fluorescent proteins. *Nat Methods* 9:727–729.
51. Young RW (1967) The renewal of photoreceptor cell outer segments. *J Cell Biol* 33: 61–72.
52. Edwards SL, et al. (2013) An organelle gatekeeper function for Caenorhabditis elegans UNC-16 (JIP3) at the axon initial segment. *Genetics* 194:143–161.
53. Li P, Merrill SA, Jorgensen EM, Shen K (2016) Two clathrin adaptor protein complexes instruct axon-dendrite polarity. *Neuron* 90:564–580.
54. Fujiwara M, Teramoto T, Ishihara T, Ohshima Y, McIntire SL (2010) A novel zf-MYND protein, CHB-3, mediates guanylyl cyclase localization to sensory cilia and controls body size of Caenorhabditis elegans. *PLoS Genet* 6:e1001211.
55. Jensen VL, et al. (2010) Localization of a guanylyl cyclase to chemosensory cilia requires the novel ciliary MYND domain protein DAF-25. *PLoS Genet* 6:e1001199.
56. Burd C, Cullen PJ (2014) Retromer: A master conductor of endosome sorting. *Cold Spring Harb Perspect Biol* 6:a016774.
57. Mukhopadhyay S, et al. (2010) TULP3 bridges the IFT-A complex and membrane phosphoinositides to promote trafficking of G protein-coupled receptors into primary cilia. *Genes Dev* 24:2180–2193.
58. Wang J, Morita Y, Mazelova J, Deretic D (2012) The Arf GAP ASAP1 provides a platform to regulate Arf4- and Rab11-Rab8-mediated ciliary receptor targeting. *EMBO J* 31:4057–4071.
59. Moritz OL, et al. (2001) Mutant rab8 Impairs docking and fusion of rhodopsin-bearing post-Golgi membranes and causes cell death of transgenic Xenopus rods. *Mol Biol Cell* 12:2341–2351.
60. Schou KB, Pedersen LB, Christensen ST (2015) Ins and outs of GPCR signaling in primary cilia. *EMBO Rep* 16:1099–1113.
61. Knödler A, et al. (2010) Coordination of Rab8 and Rab11 in primary ciliogenesis. *Proc Natl Acad Sci USA* 107:6346–6351.
62. Lodowski KH, et al. (2013) Signals governing the trafficking and mistrafficking of a ciliary GPCR, rhodopsin. *J Neurosci* 33:13621–13638.
63. Berman DE, Ringe D, Petsko GA, Small SA (2015) The use of pharmacological retromer chaperones in Alzheimer's disease and other endosomal-related disorders. *Neurotherapeutics* 12:12–18.
64. Mecozzi VJ, et al. (2014) Pharmacological chaperones stabilize retromer to limit APP processing. *Nat Chem Biol* 10:443–449.
65. Oikonomou G, Perens EA, Lu Y, Shaham S (2012) Some, but not all, retromer components promote morphogenesis of C. elegans sensory compartments. *Dev Biol* 362: 42–49.
66. Ortiz CO, et al. (2006) Searching for neuronal left/right asymmetry: Genomewide analysis of nematode receptor-type guanylyl cyclases. *Genetics* 173:131–149.
67. Mukhopadhyay S, Lu Y, Shaham S, Sengupta P (2008) Sensory signaling-dependent remodeling of olfactory cilia architecture in C. elegans. *Dev Cell* 14:762–774.
68. Bacaj T, Tevlin M, Lu Y, Shaham S (2008) Glia are essential for sensory organ function in C. elegans. *Science* 322:744–747.
69. Procko C, Lu Y, Shaham S (2011) Glia delimit shape changes of sensory neuron receptive endings in C. elegans. *Development* 138:1371–1381.
70. Mello CC, Kramer JM, Stinchcomb D, Ambros V (1991) Efficient gene transfer in C. elegans: Extrachromosomal maintenance and integration of transforming sequences. *EMBO J* 10:3959–3970.
71. Brenner S (1974) The genetics of Caenorhabditis elegans. *Genetics* 77:71–94.
72. Schneider CA, Rasband WS, Eliceiri KW (2012) NIH image to ImageJ: 25 years of image analysis. *Nat Methods* 9:671–675.